Mineralogical and Geochemical Assessment of the Eagle Ford Shale

Senior Thesis

Submitted in partial fulfillment of the requirements for the

Bachelor of Science Degree

At The Ohio State University

by

Harold W. Elston

The Ohio State University

2014

Approved by

Dr. David Cole, Advisor

School of Earth Sciences

Abstract

The South Texas Eagle Ford shale play is a large reservoir of oil and natural gas, and it is also among the more recent gas and oil shale plays currently being developed in the United States for hydrocarbon extraction. For this reason, the physical and chemical characteristics of the rock formation remain largely unknown outside of private corporations. The objective of this research is to determine the relative abundances of different minerals in samples obtained from 5 separate wells, and the concentration of total organic carbon (TOC) contained in them. The mineralogy is determined by X-ray Diffraction (XRD) of randomly oriented powder mounts in conjunction with Scanning Electron Microscopy (SEM) of unpolished fragments, mechanically polished thin sections, and ion milled slope cut fragments. Analysis shows that there is substantial variation in mineralogical composition among the samples analyzed, including the relative quantities and types of phyllosilicates and carbonate minerals. These data, along with data provided by Chesapeake Energy Corporation, show a relationship between TOC and the amount of illite and calcite. This relationship is also evident in the SEM images that show significant amounts of organic matter infilling the carbonate microfossils.

Acknowledgements

I want to thank Dr. David Cole for bringing me onto his team and advising me throughout the course of my research and thesis work. Many thanks go to Dr. Julie Sheets for all the hours spent helping me on the XRD, SEM, ion mill, coating samples, interpreting data, and other technical and analytical aspects of this research. All your assistance and guidance given to me throughout this study made the major portion of this thesis possible. Thanks to Dr. Susan Welch for the time spent working with me on the Picarro CRDS, the OI Analytical iTOC analyzer, for coaching me through sample prep, data analysis, and other assistance given to me throughout this project. Thank you to Mario Gutierrez, Alexander Swift and the entire SEMCAL team for their assistance and support as well. Also, thank you to Shell Exploration and Production Company for the funding that supported the initial research on this project, conducted during summer 2013 when I was a recipient of a Shell Undergraduate Research Experience internship. Thank you goes to Chesapeake Energy Corporation for supplying the samples used for this study.

Table of Contents

Introduction

The Eagle Ford shale play in South Texas is one of the largest reservoirs of oil and natural gas in the United States currently being produced (Figure 1). The first successful well was drilled in 2008 by Petrohawk Energy, and the success of this well spawned the multi-billion dollar boom of horizontal drilling in the Eagle Ford shale formation that is exploited today (Railroad Commission of Texas 2014).

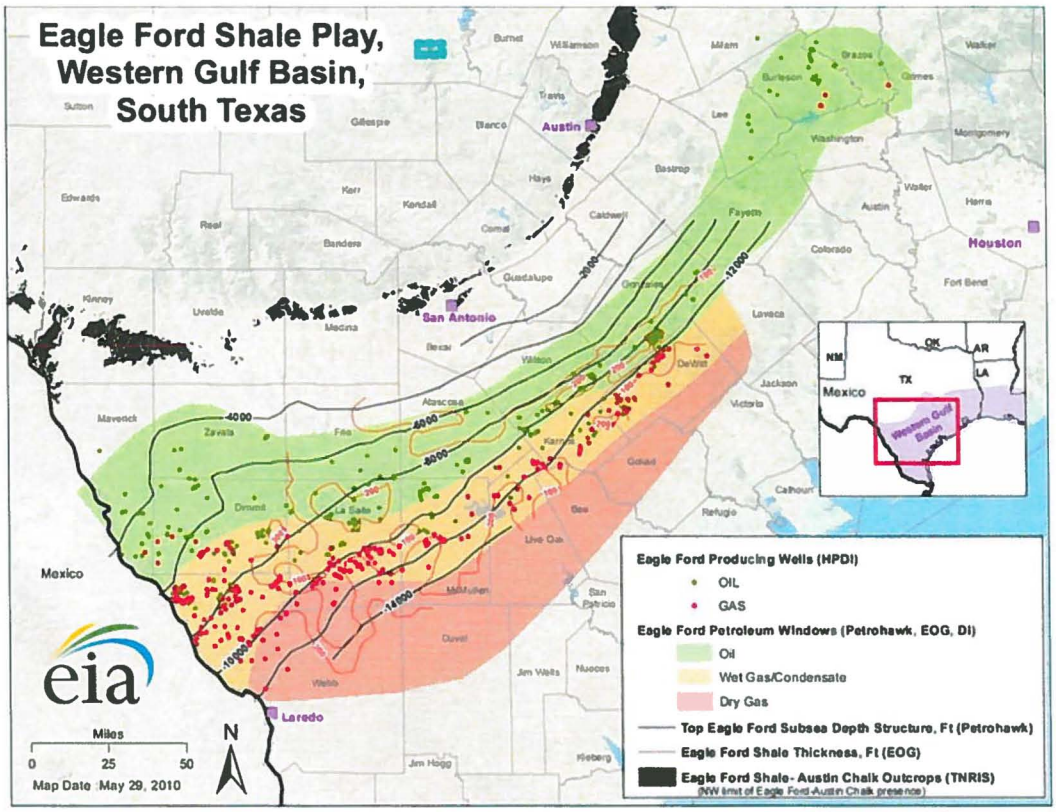

Figure 1. Map showing formation location and production areas of the Eagle Ford Shale play. (U.S Energy Information Administration)

The Eagle Ford is Cretaceous in age and lies between formations of Austin Chalk above and Buda Limestone below. The Eagle Ford is thought to be the source rock for oil and gas in the Austin Chalk formation and its rich hydrocarbon content makes it a valuable reservoir rock as well (Railroad Commission of Texas 2014). The areas where oil and gas production are the highest occur near the Karnes Trough area in Karnes County Texas, and the Hawkville Field area in LaSalle and McMullen counties as depicted in Figure 2 (Martin et al. 2011). The formation can be observed as an outcrop in the old town of Eagle Ford Texas, present day Dallas area, and this outcropping location is where the formation got its name. From the point of outcrop, the

formation becomes increasingly deeper to the southeast, and maturity of the play increases from the northwest to the southeast along with the depth (Bryndzia and Braunsdorf 2014). In the areas of present day oil and gas production, the depths of the play range from 1,500 ft to 14,000 ft with a thickness of 50 ft to the NE and 330 ft to the SW (Martin et al. 2011).

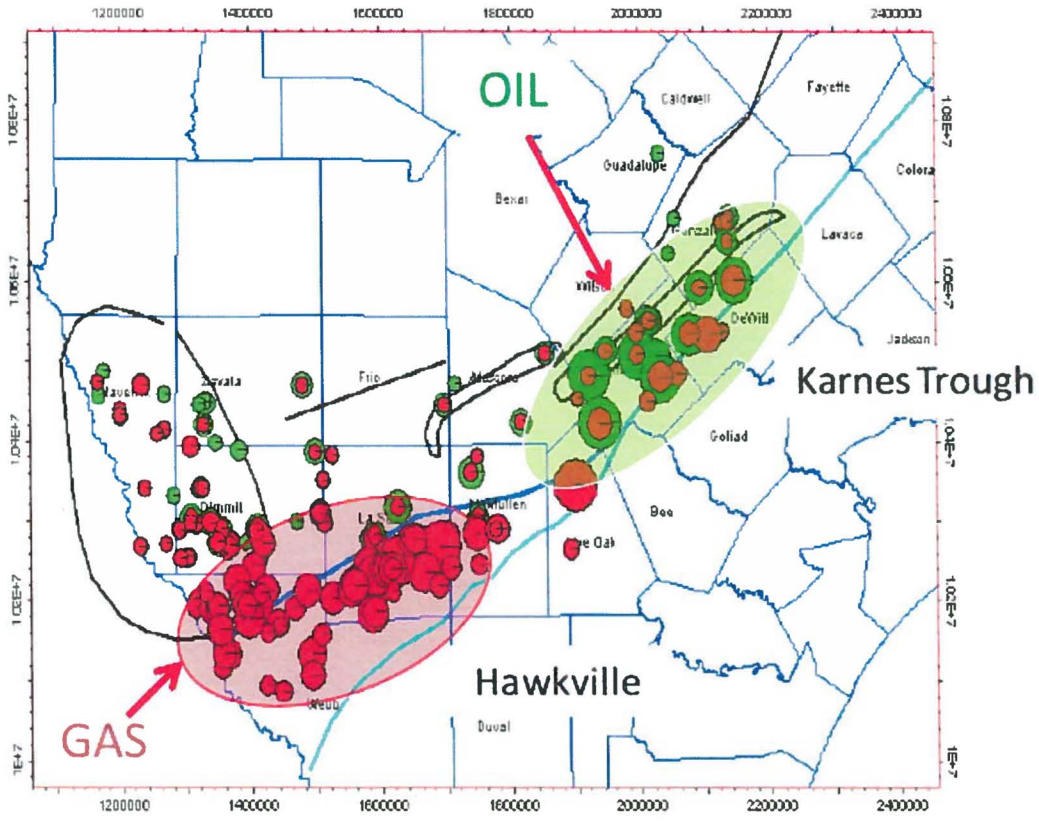

Figure 2. Locations of the highest oil and gas productions in the Eagle Ford play. (Martin et al. 2011)

New developments of oil and gas fields are important. By exploiting our own energy resources in the United States we can reduce our dependency on foreign oil, and at the same time generate a major boost to our nation's economy. For economic and environmental reasons, furthering our understanding of the major shale deposits within the United States is important to us as a nation.

Goals and objectives

The overall goal of this research was to explore the relationship between the mineralogical and geochemical composition of samples from the Eagle Ford Shale gas and oil play. To accomplish this, the specific objectives focused on were mineralogy, and weight percentages of total organic carbon in the rock samples. The hypothesis being tested for the Eagle Ford formation is that there exists a correlation between one or more mineral phases present, such as clays and carbonates, and the percentage of total organic carbon in the rock.

1. The first objective was to determine what minerals are present and their approximate weight percentages.
2. The second objective was to develop effective ion milling protocols to better prepare the shale samples for SEM observations.
3. The final objective was to analyze the data to determine whether or not the hypothesis of an existing correlation between the mineralogy and total organic carbon was supported.

Methods

Geologic Materials

The Chesapeake Energy Company provided 10 of their Eagle Ford core samples from 5 different counties in southeastern Texas to The Ohio State University for research purposes, and these samples were utilized for this study. The facilities in the Subsurface Energy Materials Characterization and Analysis Laboratory (SEMCAL) in the School of Earth Sciences were used to study them in detail.

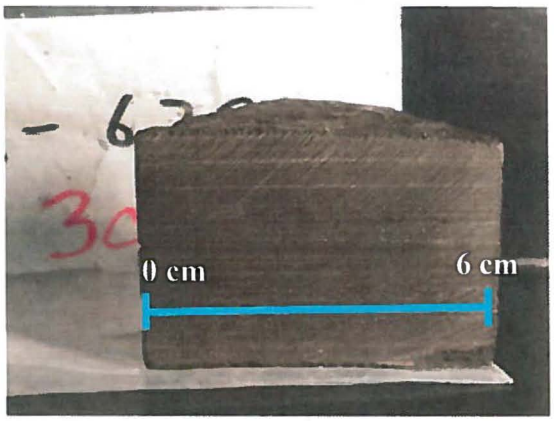

Figure 3. Original sample size of EF 30 with visible layers in the sample.

The core samples measured anywhere from 6—8 cm L, by 5—6 cm W, by 2—3 cm H (Figure 3). The samples were noticeably different shades of gray to black and all of them had visible white calcite rich layers running horizontally through them. There were also pyrites seen easily with the naked eye or under a reflecting light microscope in pieces of partial core.

The ten samples were taken in pairs from wells in five different South Texas counties (Figure 4). The data from Chesapeake show all the samples to be relatively carbonate rich. The only sample with substantial amounts of clay is EF 29 with 40.4% of the rock consisting of clays (Table 1).

EF Sample Number	Total Carbonate % ($CaCO_3$ + TOC)	Total Non-Clay Fraction %	Total Clay Fraction %	Depth (Ft)	Location (County in Texas)
22	89.9	97	3	8747	La Salle
23	77.2	88.2	11.8	5512	Zavala
24	58.8	78.9	21.1	5701	Zavala
25	50.5	77.3	22.7	6330	Dimmit
26	84.4	95.6	4.4	6366	Dimmit
27	85.9	96	4	7923	Webb
28	44.3	73.1	26.9	8139	Webb
29	26.8	59.6	40.4	6260	Frio
30	63.3	78.2	21.8	6299	Frio
31	56	78.1	21.9	8801	La Salle

Table 1. Sample location, with total carbonate and clay vs. non-clay fraction percentages of each sample. (Data provided by Chesapeake Energy Corp).

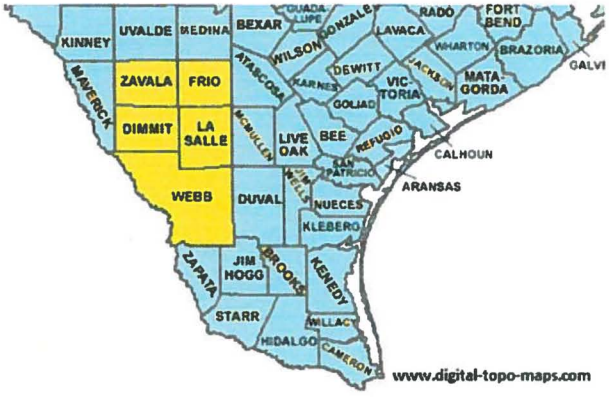

Figure 4. Map of the counties where the samples were taken from in southern Texas. A pair of samples was taken from one well in each of the five counties. (Location information provided by Chesapeake Energy Corp).

X-Ray Diffraction (XRD)

In order to get the most accurate X-ray scan, bits of the sample being measured were crushed into a fine powder. To gain these small chips of rock from the larger hand samples, each one was loosely wrapped in clear plastic wrap. A hammer was then used to strike one of its edges, efficiently breaking off small chips of the rock. This method works well for a few solid blows, but the plastic wrap began to disintegrate at the location of impact rather quickly. The plastic wrap kept the small chips contained in one small easily controlled space and did not contaminate the sample.

The smaller bits of rock and powder were then collected and crushed with a ceramic mortar and pestle. The larger bits of rock were easily broken down by light taps of the pestle. A steady amount of pressure and rotation were all that was needed to eventually render the small bits of shale into a finely ground powder with the desired consistency for measurement in the XRD. This powdered rock was then placed and compacted tightly into the stainless steel XRD sample holder (Figure 5), which was then placed into the XRD for analysis.

XRD employs the diffraction of X-rays from a mineral's crystal structure to aid in the identifying of the mineral. Every mineral has a unique crystalline structure that interacts with electromagnetic radiation in different ways. This orderly periodic arrangement of atoms in the crystals allow them to be identified using X-rays (Moore and Reynolds 1989).

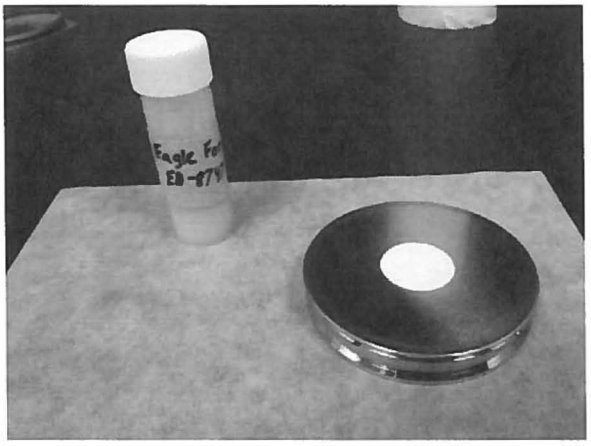

Figure 5. XRD sample holder with sample.

The results were analyzed using PANalytical HighScore with Plus option software to compare the peaks representing d-spacings of interatomic planes. The XRD manufacturer PANalytical claims the HighScore Plus software is a complete powder analysis program that performs phase identification and crystallographic analysis; groups the data into clusters and characterizes them (PANalytical 2014). The program then matches profiles of mineral peaks found with XRD, and identifies each mineral using the software's suggested matches. An example of the graphical output is shown in Figure 6.

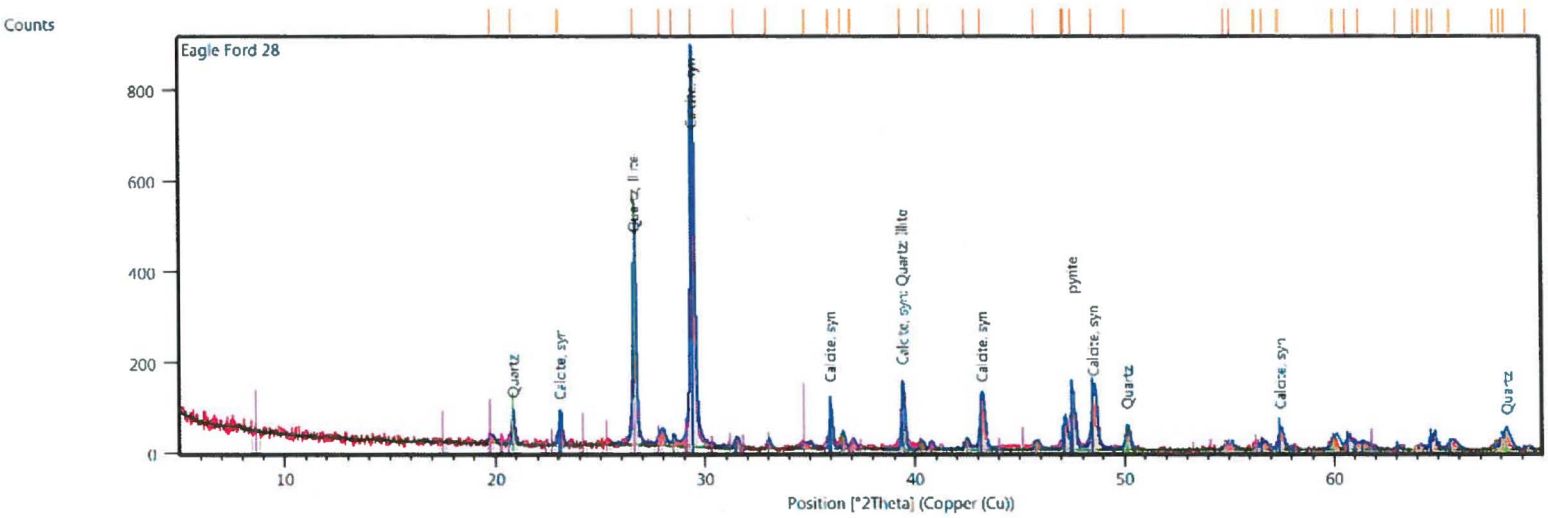

Figure 6. XRD results for EF 28. Not all of the peaks get a label by the software as seen above. The user can determine these smaller peaks by matching their d-spacing with the corresponding mineral.

Basic knowledge of the formation history of the rock is needed in order to make accurate interpretations of the data. For example, the software was showing that chalcopyrite ($CuFeS_2$) was present in many of the samples when only pyrite (FeS_2) was present. This was confirmed on the SEM by testing the pyrites in the sample using the microscope's energy dispersive spectrometer (EDS), which detected no traces of copper in the FeS2.

Sample Preparation

The major tool used in the SEMCAL lab to prepare a high quality surface for viewing with the SEM was the Leica EM RES102 ion beam milling system. Mechanical methods of milling a flat surface can pluck grains from it, leaving false pits or pores resulting in an incorrect interpretation of the rock's pore and surface structure. Mechanical methods can also cause smearing on the sample surface, especially for soft clays, which distorts the way the rock appears under high magnification. The ion mill considerably reduces these effects by slowly shaping the surface of a sample by removing ions from it using electrically charged argon gas to "blast" small but uniform amounts of material from the surface. While the end results of the ion milling process are much better than manual grinding methods (Appendix Figure A1 and A4), a good mechanically smoothed surface is an ideal surface to start with before starting the ion milling process.

The slope cut procedure was the method of choice for preparing the Eagle Ford shale samples for most SEM observations (Figure 7). However, before the samples were placed in the

ion mill they needed to have a relatively smooth surface, so that the process of milling would be much more effective. In order to get the desired surface, a small piece of each sample, measuring approximately 0.8cm in length and 0.4cm in height, was carefully prepared.

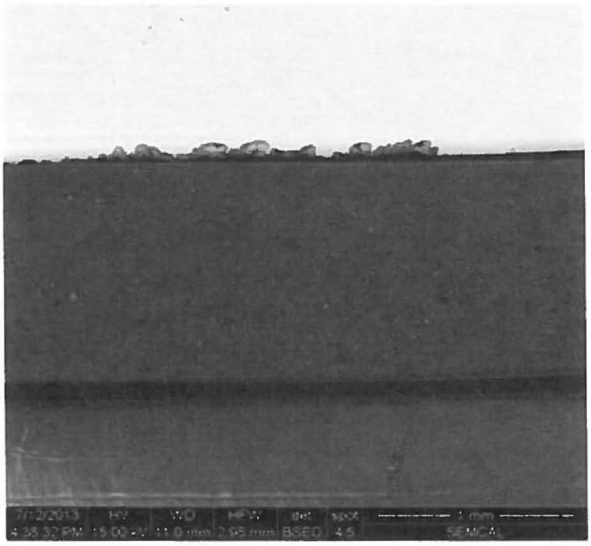

Figure 7. Image of an ion mill prepared surface taken with SEM. Sample EF 28.

This preparation was done by hand polishing the samples using a few different techniques. The first step in preparing the sample was to find a small chip that was close to the desired size. Then to get the desired dimensions, 800grit sandpaper was used to shape the rock sides and to start an initial surface. After the sample was shaped in this manner, the desired surface was worked to a progressively greater polish by using increasingly finer sandpapers. The surface was prepared using 800 to 1,000 to 1,200 to 2,400 to 4,000 grit sandpapers. After flattening and smoothing the surface as much as possible with the larger grits, a final stage of polishing with 4,000 grit was conducted. The 4,000 grit effectively polished the rock and made the surface shine under reflected light. The sample was then ready for ion milling.

After each run in the ion mill the samples were viewed using a Leica DMS 1000 digital light optical microscope. As the sanding progressed and a few samples had been prepared, a peak in the center of the surface was noticed with the SEM (Figure 8). This peak would influence the ion milling process by keeping the sample from being polished on the far side of the peak from the sample holder's mask.

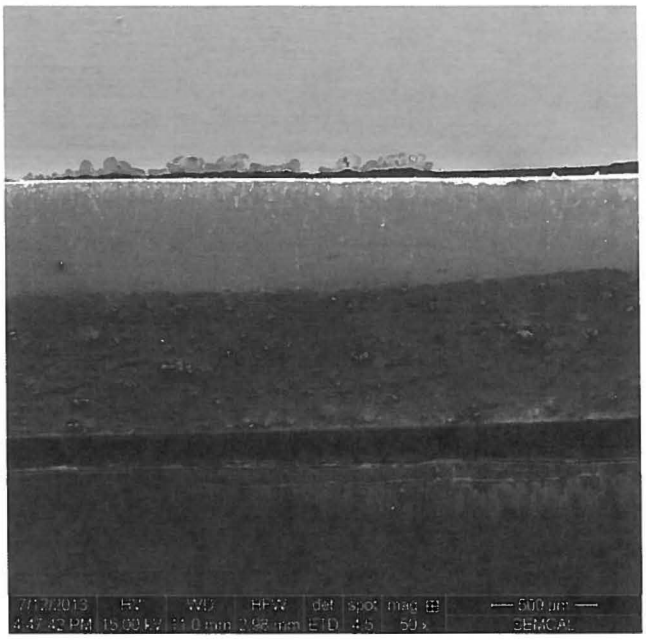

Figure 8. SEM view of Ion milled sample with ridge from hand sanding visible.

After studying this problem it was determined that the motion of sanding performed on the sample led to this peak. The samples were too delicate to pinch with pliers (the rock would break), and they were also too awkward to place on a mechanical polisher, so they were held and polished by hand. Because the samples were quite small and hard to hold onto, the sample would shift slightly back and forth with the polishing motion of the hand, causing uneven sanding, and resulting in the ridged surface. As a result the method was changed and a circular motion was used to polish the sample, which resulted in a much better, horizontal surface.

Scanning Electron Microscopy (SEM)

To test and complement the XRD results, some of the samples were examined with a FEI Quanta 250 Field Emission Gun Scanning Electron Microscope (SEM). In order to have a clean view of the rock, small freshly broken bits of each sample were viewed on the SEM before any polishing was completed. These bits were placed on an aluminum SEM stub using double-sided carbon tape as the adhesive (Figure 9). The samples were then coated with platinum/palladium to prevent charging in the microscope (Appendix Figure A1).

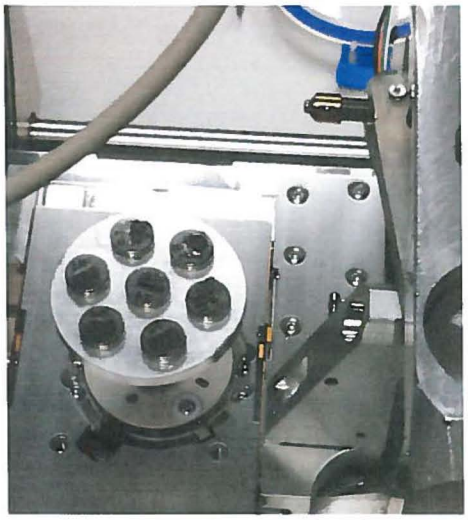

Figure 9. Coated samples on SEM stubs for ease of viewing with the microscope.

Using the microscope's energy dispersive spectrometer (EDS) different elements could be identified in the rocks (Figure A4 and A5). Using this method the type of minerals present could be determined. These bits were untouched and showed the raw, clean, broken edges of the rock, which allowed for detailed observations of the rock structure, texture, and mineralogy. After a smooth well-prepared surface was made using the Leica ion mill, the samples were then reexamined.

The purpose for obtaining such a smooth clean surface is so when viewing the rock in the SEM it appears as one homogeneous surface, one where most if not all features are at the same height in order to minimize differences in the relief. This allows the different characteristics of the rock to be seen without influence from shadows caused by an uneven surface and also helps quantify relative abundances of minerals. These samples were typically viewed using 500x—

2000x magnification. If any surface had greater relief than another, such as a group of pyrite crystals raised above a clay matrix, it would cause a shadow and distort or confuse the real image of the rock sample. Commonly manual polishing methods of preparing a smooth surface can pluck grains from the rock, creating "false pores" in the surface when viewed on the SEM. It cannot be overemphasized that a well prepared surface is crucial for accurate SEM analysis. A significant amount of time and care was devoted to this aspect of the study by employing hand polishing methods, followed with a final polishing via ion beam milling.

Results

Mineralogy

XRD

The percentages of minerals (determined by the XRD), vary among the samples analyzed; but XRD results show that the most common minerals contained in the samples are calcite, quartz, pyrite, illite and albite (Figure 10).

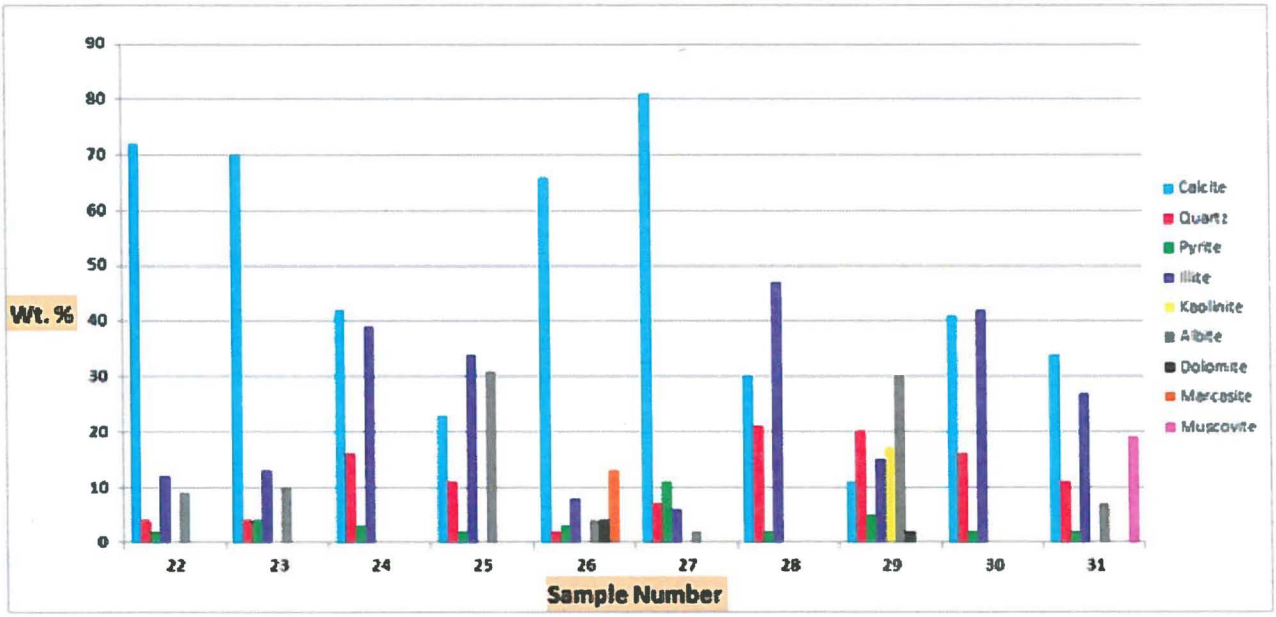

Figure 10. XRD Mineralogy of the 10 Eagle Ford samples determined in SEMCAL labs.

Other minerals found in only a few samples were kaolinite, dolomite, marcasite, and muscovite. Most of the pyrite observed in SEM images was framboidal pyrite, although other morphologies such as equi-granular were also observed (Figure 11).

Two samples, EF 29 and EF 22, exhibit distinctive differences from the others based on a comparison of XRD and SEM observations. The latter sample was measured a second time, but with different powder from the sample in order to gain more extensive results. EF 29 (depth 6,260 ft.) had eight minerals, including kaolinite and dolomite identified by the XRD, more mineral types than any of the other samples. The first XRD run of sample EF 22 (depth 8,747 ft.) consisted of only calcite and quartz, but analysis with the SEM demonstrated both pyrite and albite present, but in small quantities possibly not detectable by XRD in the first portion of sample ran. When a second run of EF 22 was conducted the XRD showed the presence of albite, pyrite, and illite in addition to calcite and quartz, which confirmed the SEM results and similarity

to the mineralogy seen in the other Eagle Ford samples. Another study has also found this same general mineralogy of quartz, calcite, pirite, illite, and other clays in the Eagle Ford formation (Mullen et al. 2010). This is one example of how sample heterogeneity can have an effect on analysis of the rock, as its mineralogy can vary across the sample. Also the XRD cannot detect phases below 3—5% in abundance. These are some reasons why it is beneficial to utilize the SEM in tandem with the XRD, so a more thorough assessment of the rock can be made.

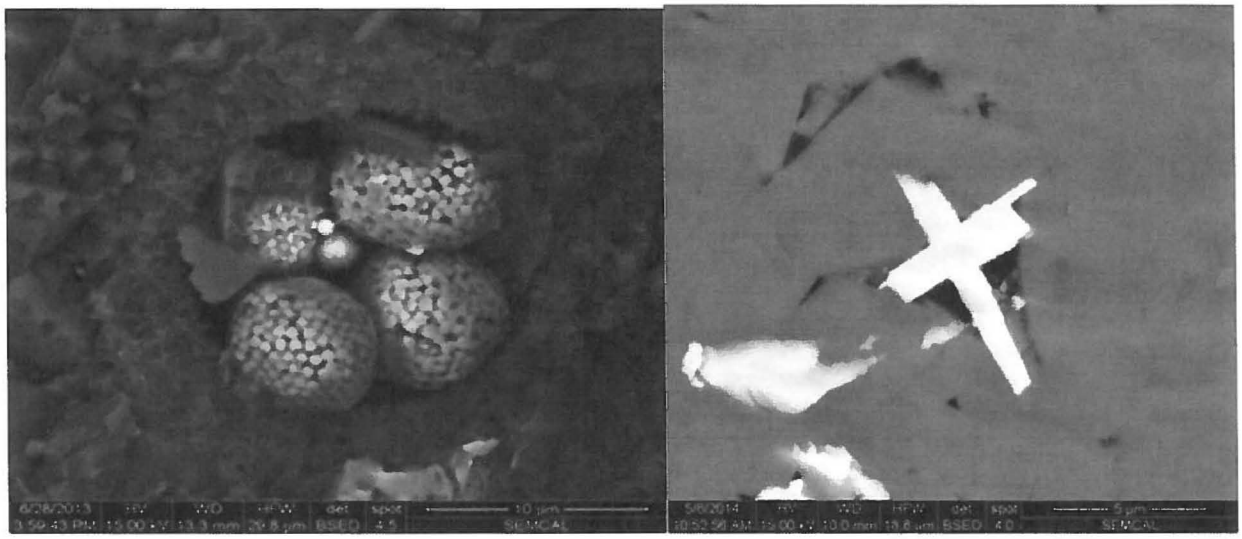

Figure 11. Framboidal and other morphologies of pyrite crystals were found in sample EF 27 and in the other samples as well.

Ion Milling

After hand polishing, the sample was then set in the ion mill's slope cut holder, which was not a trivial task. After many runs and reruns it was determined that the holder and sample had to be setup with precision. The mask on the slope cutting holder must line up with and be parallel to the top of the two arms on the holder (Figure 12). The sample has to be placed on the copper specimen carrier, which was accomplished by using double sided adhesive tape (Figure 13). The use of hot wax is recommended by the manufacturer, but tape was utilized to prevent any possible sample contamination. As a side note an attempt was made to affix a shale sample to the appropriate holder with wax as recommended by the manufacturer, but this was unsuccessful due to the high temperatures generated by the milling process which melted the wax, causing the sample to fall into the milling chamber.

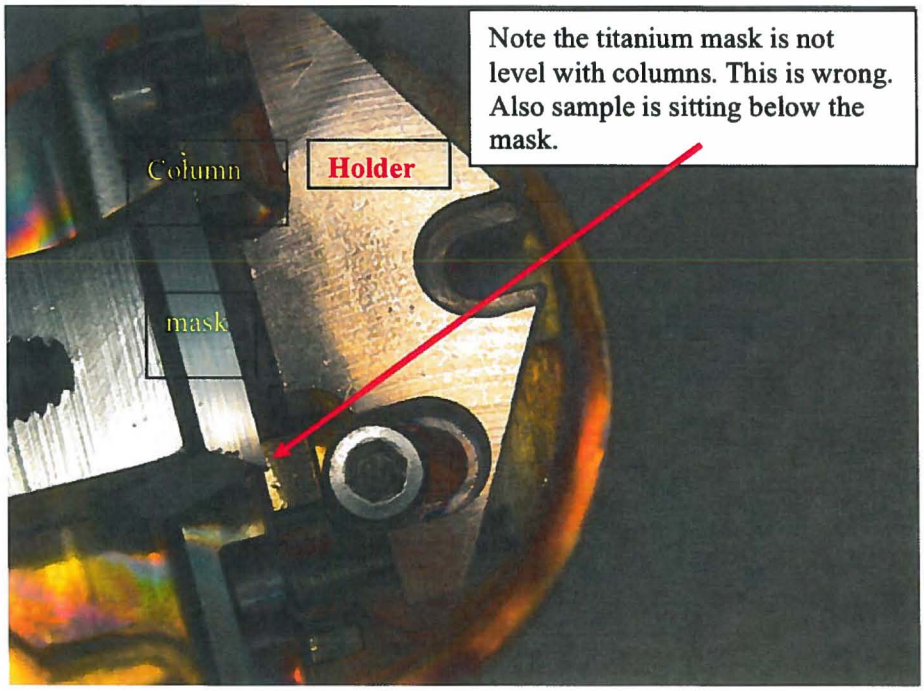

Figure 12. First ion milling attempt; EF 29 after being milled for 1 hour. Sample was to low and had been milled in wrong direction, which resulted in copper being displaced on the sample from the holder. Also the sample is sitting below the mask, when it needs to be just above it.

Both copper and carbon tape were used, with the carbon tape exhibiting adequate adhesive qualities, thus yielding the best results. With the sample firmly attached to the carrier it then had to be placed on the holder in such a way that the surface for milling was just barely above the top of the mask (Figure 14). In order to position the sample correctly the cutting holder was placed in the fixing block, which allows for the raising and lowering of the specimen carrier for the most accurate adjustments.

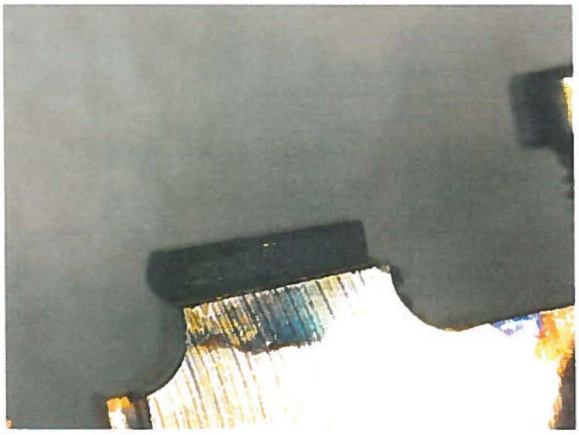

Figure 13. Sample stuck to copper holder with double sided copper tape.

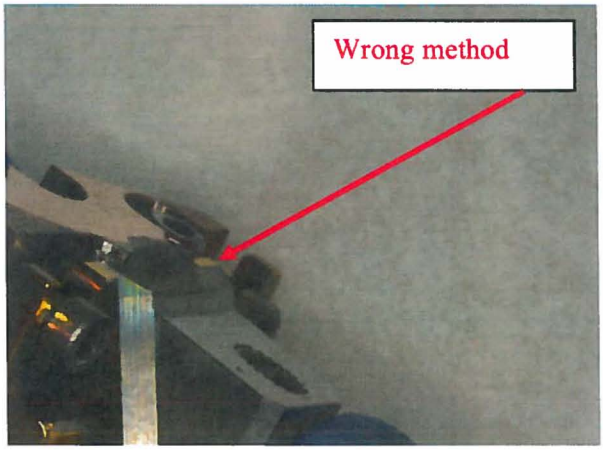

Figure 14. Here the sample is too high, and the mask is too tight digging into it. This will cause the sample to break apart.

The positioning of the sample was checked using a Leica DMS1000 light microscope, and once the placement was satisfactory the sample was milled. The conditions for each run can be seen in Table 2. The first run on EF 29 produced an excellent surface and no further runs were done on it. EF 28 was slightly rough and looked unfinished after its first milling but a second milling resulted in a good surface. The improvements here can be attributed to the extra amount of milling time for the second run.

Sample ID	Ion Mill Run #	High voltage (kV)	Gun current (mA)	Gun angle (degrees)	Milling angle (degrees)	Gun tilting (degrees)	Milling time	Notes
EF29	1	10.0	3.5				1 hour	
EF28	1	8.0	3.2	2.0			1hr 13min	
EF28	2	8.0	3.3	3.0			2 hours	
EF27	1	5.5	2.3	5.0	5		3 hours	not good run, bad surface
EF27	2	6.0	2.5	2.5			1 hour	
EF27	3	1.5	1.0	10.0	10		10min	slope cleaning run
EF26	1	7.5	3.0	3.0			3 hours	
EF22	1	7.5	3.0	3.0	3		2 hours	

Table 2. Ion mill run parameters for each run successfully completed on the samples. (Missing data was not recorded)

The initial run on EF 27 did not produce a clean smooth surface. There were visible wave and cone-like structures across the milled area from either bad sample preparation or bad milling, and it was not ideal for viewing in the SEM (Figure 15-A). This was the only sample that had these structures, which may have been caused by the high gun angle (5°), or a worn out mask on the SEM sample holder that was used for the first run on EF27. The edge on the mask was unevenly worn down, possibly causing the milling process to be uneven and the surface to be bad. To fix the sample, the surface was re-polished with 4,000grit sandpaper, the mask was rotated to a fresh edge, and the gun angle was decreased.

This second run produced a much better surface area. For a final touch, a slope cleaning (program built into the ion mill) was performed on EF 27 for 10min (Table 2), and it was then coated with platinum/palladium to prevent charging in the SEM. This produced an excellent surface for viewing (Figure 15-B).

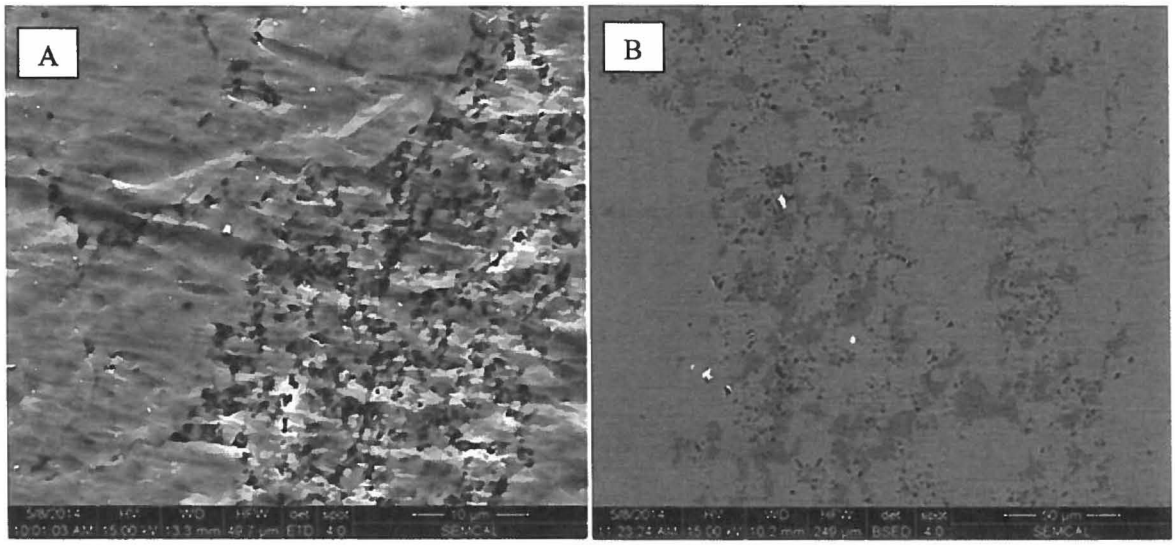

Figure 15. (A) EF 27, rough, wavy surface after first run on ion mill. (B) Second run and slope cleaning. Shows a very good surface of pores and contrast between clay and calcite. There are noticeable scratch marks from the large grained sandpaper used to prep the surface indicating a smaller grit size should be used.

Another noticeable problem was deep cuts or striations at certain points on the finished surfaces of the samples that were visible during observation with the SEM. This was determined to be from large grains gauging the surface from the coarse 800grit sandpaper. For future sample preparation, a higher grit number (finer grit size) such as 1,000grit or 1,200grit should be used to start shaping the desired milling surface to alleviate the deep gouges that remained, even after further sanding and ion milling were conducted.

SEM of Broken Chips

The SEM was used to examine the natural, three dimensional textures of surfaces of the samples before they were polished mechanically or ion milled. Cleanly broken chips were viewed on the SEM, which revealed numerous fossil types in all the samples (Figures 16), and allowed for an examination of the structure of the rock before being milled. The calcite microfossils were predominately coccolithophores and foraminifera and were visible throughout the rock samples.

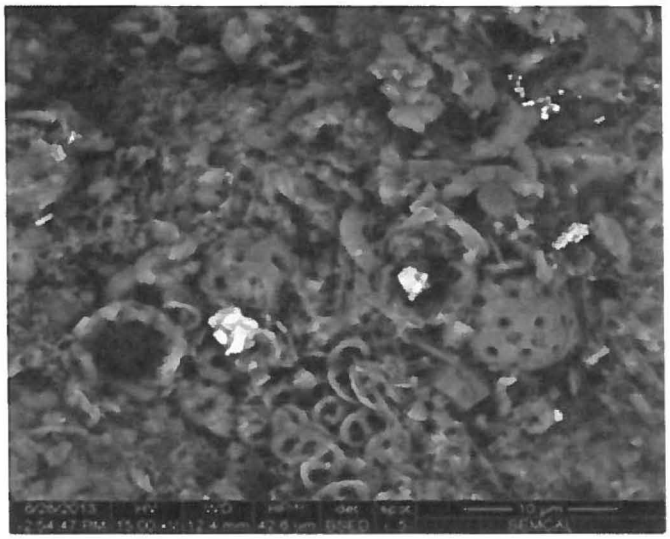

Figure 16. EF 28 Coccolithophores, fossils, found by inspection with the SEM.

The samples with the most mineralogical diversity were EF 29 and EF 26, which contain 8 and 7 different minerals respectively. The structure of the clay minerals and nature of pores in the rock were also apparent in certain samples (which will not be discussed in this work). In other samples there were patches of organic carbon visibly present in large quantities (Figure A2), which will be discussed further in the following section.

Carbon Content

As is expected with marine sedimentary shale, these samples consisted of measurable quantities of carbon. The goal was to determine what type of carbon was present, organic versus inorganic. A color contrast in dark vs. lighter gray was noticed among some carbon bearing phases (Figure 17-A) while viewing with the SEM, and it was determined that the darker carbon was organic by using the EDS analysis (Figure A4 and A5).

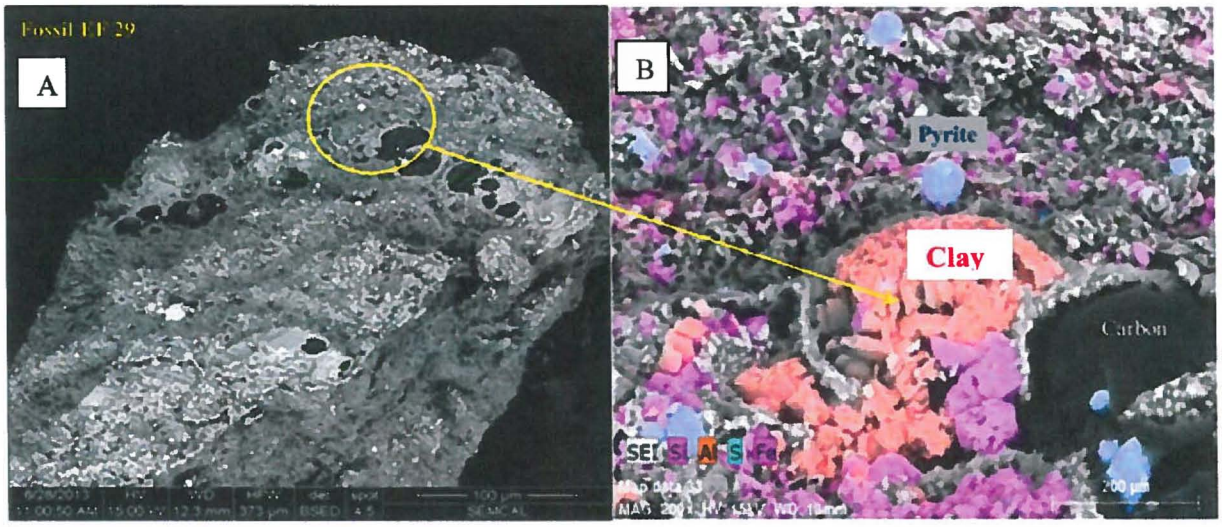

Figure 17. Organic carbon and clay in proximity with a fossil in EF 29

Microfossils are also present in samples of EF 29 and EF 28 and most of the organic carbon was found in close proximity to these fossils. A majority of the fossils observed in the rock had the organic material deposited inside and around the fossils structure (Figure 17-B). This can also be observed in the fossils that have been split and polished with the ion mill (Figure 18).

This type of black organic carbon still in its solid form is called kerogen, and is exactly what oil and gas companies want to see in the rock when drilling into a formation. Kerogen is hydrocarbon material that has not yet been heated (cooked) into its liquid form of oil or gas condensates. The abundance of kerogen in these samples shows that there may be potential oil and gas in the Eagle Ford as one goes deeper into the formation. As shown in Figures 1 and 2, the shallower depths contain oil, and the deeper areas in the play are progressively gas rich as the play dips downward. The increasing depth causes the hydrocarbons to be subject to higher temperatures, resulting in more gas being produced.

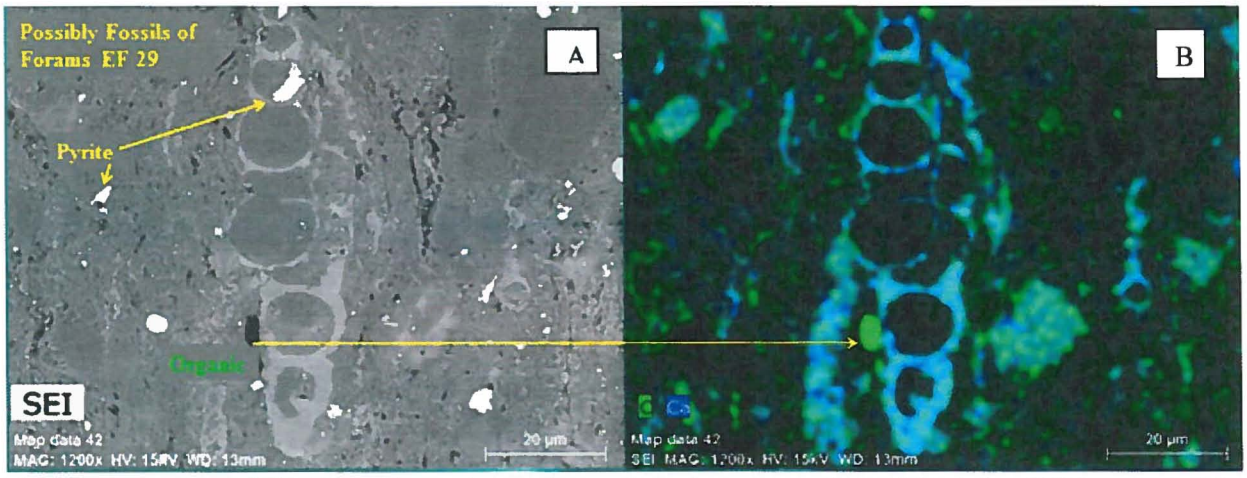

Figure 18. Images of EF 29 fossils, pyrite, and organic carbon were taken while doing SEM analysis. The TOC is in close proximity to the fossils. Picture B shows the TOC using SEM's EDS carbon and calcium map.

The average vitrinite reflectance (Ro) values included in the Chesapeake data sheet show that the formation sediments become more mature in the southern counties of Webb and La Salle. The maturity of the organic matter within a formation can be determined by vitrinite reflectance as vitrine (a type of woody kerogen) is sensitive to temperature changes (Wust et al. 2013). The vitrinite maturity for these samples increases with the Eagle Ford as it dips deeper into the subsurface in the southernmost counties which can be seen in Table 3 and the map used back in Figure 4. Geographically this is where the formation is found at depths deep enough for the organic carbon to be heated to the maturation temperatures adequate for generating oil and gas (Table 3).

EF Sample Number	Average %Ro (Maturity)	Depth (Ft.)	Location (County)
29	0.58	6260	Frio
30	0.58	6299	Frio
23	0.77	5512	Zavala
24	0.77	5701	Zavala
25	0.96	6330	Dimmit
26	0.96	6366	Dimmit
31	1.18	8801	La Salle
22	1.18	8747	La Salle
27	1.57	7923	Webb
28	1.57	8139	Webb

Table 3. The %Ro values for the ten samples. The higher the Ro, the more mature the sediment. Webb and LaSalle counties are buried the deepest in this sample set and are therefore the most mature. (Data provided by Chesapeake Energy Corp.)

Correlation of Mineralogy and TOC

The mineralogy results obtained from XRD and SEM were compared to the TOC data provided by Chesapeake, yielding noticeable trends. It was observed that the weight percent of TOC in the samples seem to fluctuate according to the weight percent of illite in each sample. The samples with low illite percentages (the impure limestone's), such as EF 22, 23, 26, and 27, tend to have low TOC, while the samples with higher illite percentages (the more carbonated clay-rich muds) have moderate to high TOC (Figure 19 and 20).

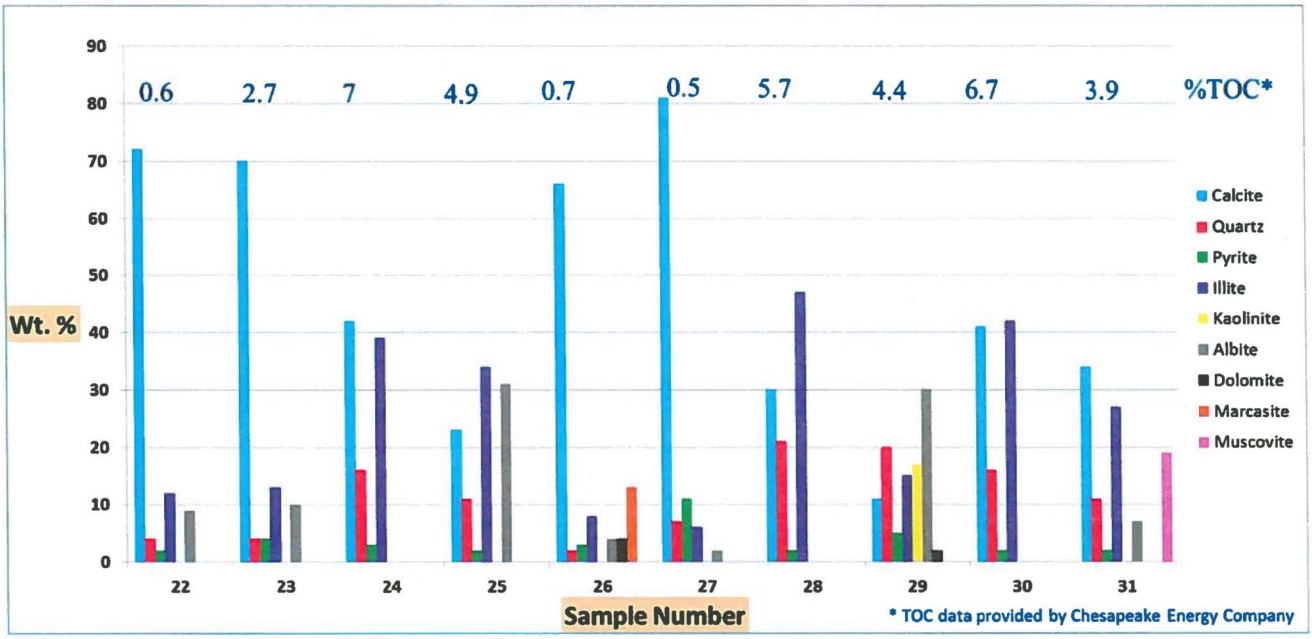

Figure 19. Mineralogical and TOC data of samples. Generally the TOC wt. percent increases with increasing illite wt. percent.

According to the Chesapeake data the samples with the highest organic carbon are EF 24, and EF 30. In both of these samples the weight percent ratio is roughly 40/7 illite/TOC. This trend of high illite percentages correlating with high TOC percentages is seen throughout the data when testing the hypothesis with analysis of variance (ANOVA) (Figure 22 and 23).

Another trend that seemed to be present in the samples is the relationship of calcite and illite. When calcite is enriched in the rock illite appeared to be lower in abundance and vice versa (Figure 21). However, while these two correlate with each other more than other minerals in the samples, analysis shows that there is only a week correlation between the two minerals and not a major one as first perceived (Figure 22 and 23). The average mineral abundance and TOC of all the Eagle Ford samples indicate that the samples are relatively high in calcite (47%), and illite (24.3%)

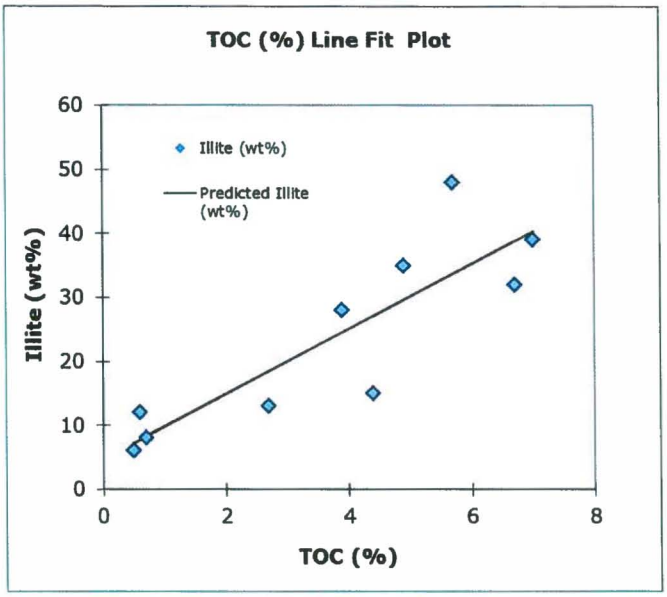

Figure 20. Illite plotted against TOC. A general trend showing TOC percentage increasing with a higher percent of illite in the samples. (TOC data from Chesapeake Energy Corp.)

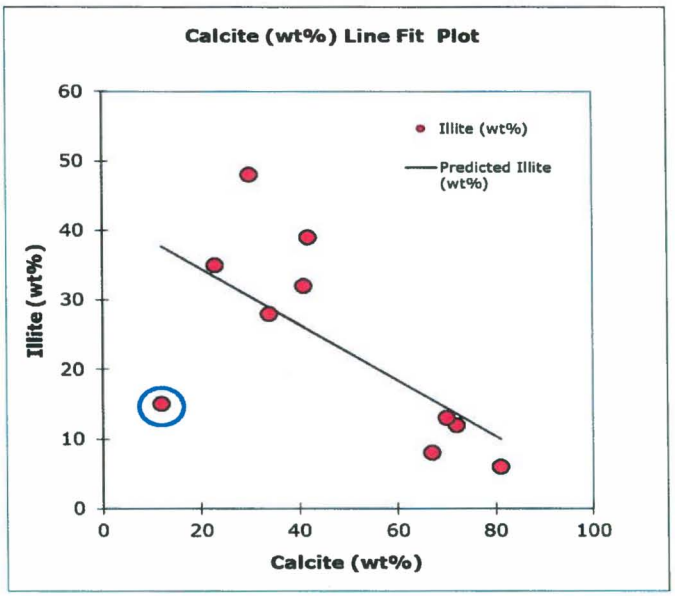

Figure 21. This plot shows the relationship of calcite and illite in the samples. Sample EF 29 (circled in blue) is the only one that deviates from the general trend which may be contributed to its high content of other minerals found in the sample and its location in the formation.

compared with the other minerals, and also shows a relatively high percentage of TOC at 3.71% overall (Table 4).

For those samples that are high in TOC (~5% or greater highlighted in green), there is a higher average percentage of illite (40.5%) and moderate amounts of calcite present at 34%. For those samples with low TOC (less than 4.9% highlighted in pink) the correlation of calcite/illite switches to 55.67/13.5% respectively.

Illite vs. TOC	*Coefficients*	*Standard Error*	*t Stat*	*P-value*	*Lower 95%*	*Upper 95%*
Intercept	4.7507	4.6029	1.0321	0.3322	-5.8638	15.3651
slope	5.0807	1.0468	4.8535	0.0013	2.6668	7.4946

Calcite vs. Illite	*Coefficients*	*Standard Error*	*t Stat*	*P-value*	*Lower 95%*	*Upper 95%*
Intercept	42.5209	8.7114	4.8811	0.0012	22.4324	62.6094
slope	-0.4009	0.1667	-2.4047	0.0429	-0.7853	-0.0164

Figure 22. P-value shows a good correlation exists between illite and TOC at 0.33, and a poor to no correlation between calcite and illite at 0.0012. (pers. comm. Prof. Anne Carey)

Illite vs. TOC Regression Statistics	
Multiple R	0.8640
R Square	0.7465
Adjusted R Square	0.7148
Standard Error	7.8131
Observations	10

Calcite vs. Illite Regression Statistics	
Multiple R	0.6477
R Square	0.4196
Adjusted R Square	0.3470
Standard Error	11.8225
Observations	10

Figure 23. R^2 value shows the highpothosis that illite correlats with TOC rather well but shows a poor to no correlation between calcite and illite. (pers. comm. Prof. Anne Carey)

EF Sample Number	Calcite	Quartrz	Pyrite	illite	Kaolinite	Albite	Dolomite	Marcasite	Muscovite	TOC	Depth
22	72	4	2	12		9				0.6	8747
23	70	4	4	13		10				2.7	5512
24	42	16	3	39						7	5701
25	23	11	2	34		31				4.9	6330
26	66	2	3	8		4	4	13		0.7	6366
27	81	7	11	6		2				0.5	7923
28	30	21	2	47						5.7	8139
29	11	20	5	15	17	30	2			4.4	6260
30	41	16	2	42						6.7	6299
31	34	11	2	27		7			19	3.9	8801
Averages:	47	11.2	3.6	24.3	17	13.29	3	13	19	3.71	

Table 4. Weight percent of mineralogy and TOC Data collected for all samples with averages shown. (Mineralogy obtained by XRD in SEMCAL; TOC and depth data from Chesapeake Energy Co.)

In general these data show when there is a high concentration of organic carbon, the weight percent of clay will also be high in the rock. When the organic carbon is low in abundance, the weight percentage of calcite is much higher than that of the clay. For these Eagle Ford samples TOC is highest in the clay-rich rock.

Discussion

The goal for this thesis was to determine the relationship between mineralogy and organic carbon content of the rock samples. While relationships were found among illite, calcite, and TOC, these findings are only relevant for the small amount of each sample examined. The core samples came in hand size chunks or smaller, which then had small pieces removed from them to complete this study. This limited sample size may prevent the results reported in this work from being quantitatively applicable at longer length scales. However, the findings from these 10 Eagle Ford samples are similar to what others have reported in the literature, making these new results a reasonable approximation of the formation's over all characteristics.

These results aare similar to those of Quirein (Quirein et al. 2012) who studied wells in the same Texas counties where the Chesapeake samples were taken. They observed averages of 57% calcite, 18% illite, and 4% TOC (Quirein et al. 2012), whereas this study found 47% calcite, 24% illite, and 3.71% TOC. They did not indicate the use of SEM or XRD, but rather relied on geochemical logging tools and techniques to determine the formations characteristics.

In a conference paper titled "Understanding Production from Eagle Ford- Austin Chalk System" the authors state that the mineralogy consisted of "20% quartz, 50% calcite, 20% clay, and 10% kerogen" that they determined using only two different wells. They also claim that the formation varies little across the play, but there are slight differences in its mineralogical contents from place to place (Martin et al. 2011). This slight mineral variation is seen in the samples used in this study as well.

Two aspects that were less documented in papers focusing on mineralogy and organic carbon are the presence of microfossils and the noticeable amount of organic carbon that is found inside and surrounding their structures. These organisms are indicative of the depositional environment of the Eagle Ford formation. Formations dominated by black, calcareous, organic rich shales are indicative of a deep, quiet, anoxic marine environment with minimal disturbances from waves, which effectively protect the organic material from decay. Foraminifera of the type observed in these samples feed on the organic material from which hydrocarbons are produced, and the coccolithophores contribute to the organic matter, making their presence in the rock an important clue to the abundance of organic material present during the deposition of the Eagle Ford formation. As the formation dips further and deeper toward the Gulf of Mexico, the increasing depth results in less oil and more gas being generated as the high temperatures

continue to cook the hydrocarbons into gas. In the area where these samples were taken, there is a range of both oil and gas presence, but is typically a gas-rich environment overall.

There are also different types of clays present in the samples, such as the very minor amounts of kaolinite, and smectite (sample EF 29). However, all samples contain large amounts of illite. Many of the fossils have one or more of these clays deposited inside their structures, which can be best observed in the fossils that have been split during polishing (Figure A3). The presence and distribution of these clays can tell much about the formation that holds them. Kaolinite is generally deposited at the mouth of river systems (Potter et al. 1980), and is prevalent in near-surface environments where oxygenated conditions lead to the removal of metals during the weathering process (Keller 1956). Kaolinite is found in decreasing amounts as the temperatures increase during burial, and its absence in these samples indicates a deeper depositional environment (Weibel 2004). The only sample where kaolinite and smectite were observed was core sample EF 29, which was obtained from Frio County, located higher in the northwest portion of the formation at shallower depths.

Illite is a clay that breaks down easily in acidic environments so preservation of illites indicate that there was a near-neutral pH anoxic environment and/or quick burial during the deposition of the formation (Keller 1956), which is also important for preserving organic carbons. Illite also becomes more prevalent as the temperatures exceed 105° Celsius (Weibel 2004), which correlates to the temperatures of hydrocarbon generation of 60° to 150° Celsius (Welte and Leythaeuser 1983). The southeastern portion of the Eagle Ford is buried more deeply than its northwestern portion providing the temperatures needed for the formation and stabilization of illite and organic carbon generation seen in these samples.

Conclusions

XRD showed calcite, quartz, pyrite, and illite to be present in all of the Eagle Ford samples provided by Chesapeake Energy. Other minerals including albite, dolomite, muscovite and smectite were found, but were confined to only certain samples tested. Failure to detect these minerals in the other samples does not mean they are not present, but shows that there are limitations when measuring a small amount of a larger hand sample and that the rock characteristics change due to location and depth in the formation.

The SEM supported the XRD results by detecting the presence of calcite, quartz, and pyrite throughout the samples. Numerous microfossils were present in the rock, and in many examples organic carbon was found in close proximity to these fossils. Much of the Eagle Ford formation is made up of carbonate microfossils and so can be classified as marl and not just a mudstone or shale (Bryndzia and Braunsdorf, 2014).

The total organic carbon of the samples correlates with the amount of illite in the samples. The samples with low illite content, the impure limestones, typically have low TOC, while the samples with high illite, the more carbonate-rich mudstones, have moderate to high TOC. There is a small inverse relationship between calcite and illite, with calcite being slightly more abundant when illite is low and vice versa, the calcite is slightly lower when illite is high.

These relationships show that the Eagle Ford contains higher percentages of total organic carbon in its clay rich areas. This balance between calcite and clay is a good indicator of why the formation is well suited for fracking to extract hydrocarbons. Too much clay will soften the rock thus inhibiting the effectiveness of the hydraulic fracturing whereas too much calcite diminishes the amount of hydrocarbons present in the rock. The high carbonate content and moderate clay content create a rock that responds well to the fracking process (Eagle Ford Shale Geology, 2014). These attributes of the Eagle Ford shale play in South Texas have kept it a major player as one of the larger reservoirs of oil and natural gas in the United States.

Recommendations for Future Work

In order to gain further knowledge of the mineralogy and carbon content of the Eagle Ford formation as a whole, including its western and northern sections, additional core samples would need to be taken over a larger area of the play and analyzed. With many oil and gas wells drilled throughout the play these cores could be collected and studied for further understanding of the rock. An analysis of the types of fossils in the Eagle Ford and the areas of the play in which they are present may help to determine the deposition history of the formation. Follow-up studies of the kerogen composition and other hydrocarbons present would shed light on the maturity of the shale and its potential for oil and gas in unexplored parts of the formation, although this is most certainly the aspect of the Eagle Ford most studied by private corporations today. Future research could address spatial and textural relationships among hydrocarbons, specific minerals and associated pores, and how the depth and temperature influence the mineralogy of each sample.

References Cited

Bryndzia, Taras L., and Neil R. Braunsdorf., 2014, "From Source Rock to Reservoir–the Evolution of Self-Sourced Unconventional Resource Plays." Elements, v. 10.4.

Eagle Ford Shale News, Marketplace, Jobs. 2014. "The Eagle Ford Shale Geology". http://eaglefordshale.com/geology/ (accessed July 2014).

Keller, W.D., 1956, "Clay Minerals as Influenced by Environments of Their Formation." AAPG Bulletin v. 40, p. 2689—2710.

Martin, R., Baihly, J., Malpani, R., Lindsay, G., and Atwood, K. 2011. "Understanding Production from Eagle Ford-Austin Chalk System", in Proceedings, Society of Petroleum Engineers Annual Technical Conference and Exhibition, Colorado, Denver. SPE 145117. http:www.onepetro.org. Web, June—July 2013.

Moore, Duane M, and Reynolds, Robert C., 1997, "X-ray Diffraction and the Identification and Analysis of Clay Minerals". Oxford University Press; 2 edition, 400 p.

Mullen, J. J., Lowry C., and Nwabuoku K.C., 2010, "Lessons Learned Developing the Eagle Ford Shale", in proceedings, Society of Petroleum Engineers, Tight Gas Completions Conference, San Antonio, Texas, http:*www.onepetro.org*. Web. June 2014.

PANalytical, 2014, "HighScore Plus The Complete Powder Analysis Tool": http://www.panalytical.com/Xray-diffraction-software/HighScore-with-Plus-option.htm. (accessed July 2014).

Potter, P. E., Maynard J. B., and Pryor W. A., 1980, "Sedimentology of Shale: Study Guide and Reference Source", New York: Springer-Verlag, 306 p.

Quirein J., Murphy E., Praznik G., Witkowsky J., Shannon S., and Buller D., 2012, "A Comparison of Core and Well Log Data to Evaluate Porosity, TOC, and Hydrocarbon Volume in the Eagle Ford Shale", in proceedings, Society of Petroleum Engineers, 10 Annual Technical Conference and Exhibition, Oct. 2012. San Antonio, Texas, http:www.onepetro.org. Web. June-July 2013.

Railroad Commission of Texas, 2014, "Eagle Ford Shale Information", http:www.rrc.state.tx.us/eagleford/ (accessed May 2014).

U.S. Energy Information Administration, 2010, http://www.eia.gov/oil_gas/rpd/shaleusa9.pdf (accessed June–July 2013).

Weibel R. 2004, "Effects of Burial on the Clay Assemblages in the Triassic Skagerrak Formation, Denmark." Clay Minerals, v. 34.4, p. 619-35.

Welte, D. H., and Leythaeuser D., 1983, "Generation of Hydrocarbons in Source Rocks", Naturwissenschaften, v. 70.2 (1983), p. 53-59.

Wust R., Hackley P. C., Nassichuk B. R., Willment N., and Brezoviski R., 2013, "Vitrinite Reflectance Versus Pyrolysis Tmax Data: Assessing Thermal Maturity in Shale Plays with Special Reference to the Duvernay Shale Play of the Western Canadian Sedimentary Basin, Alberta, Canada", in proceedings, Society of Petroleum Engineers Unconventional Resources Conference and Exhibition – Asia Pacific, November 2013, Brisbane Australia, http:www.o*nepetro*.org, Web. June 2014.

Appendix

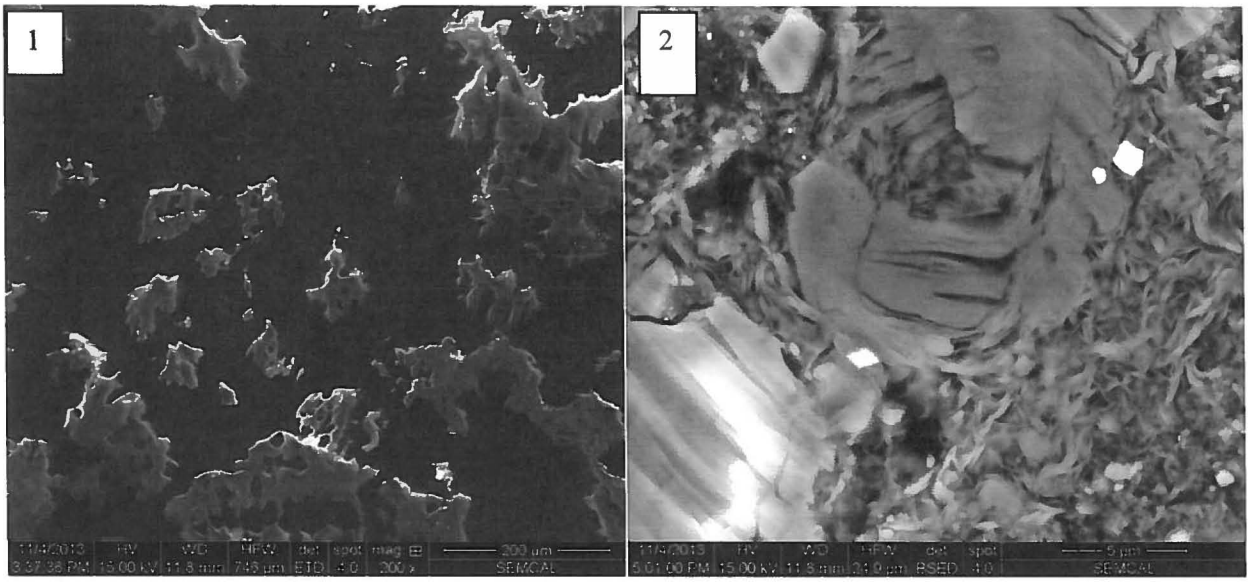

Figure A1. (1) SEM of EF 26. Uncoated with charging on surface. (2) SEM of EF 26 after ion milled and coated with platinum/palladium to prevent charging on surface; shows different clay matrix with reflective pyrites and visible pores.

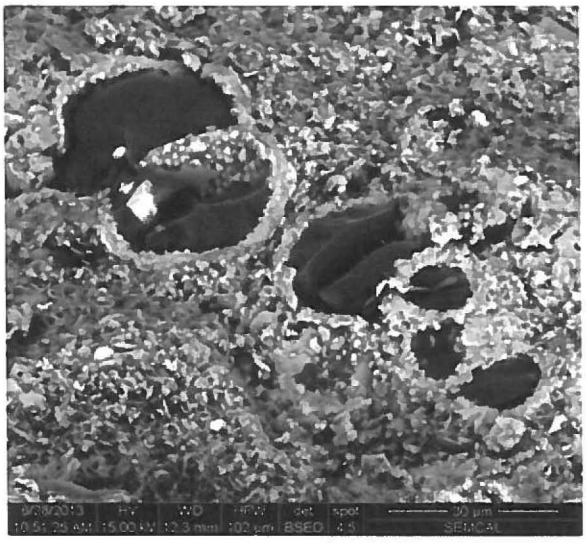

Figure A2. SEM EF 29, organic carbon in fossil, surrounded in calcite matrix

Figure A3.SEM of EF 26 after being ion milled making the properties of the curly clay to be easily seen.

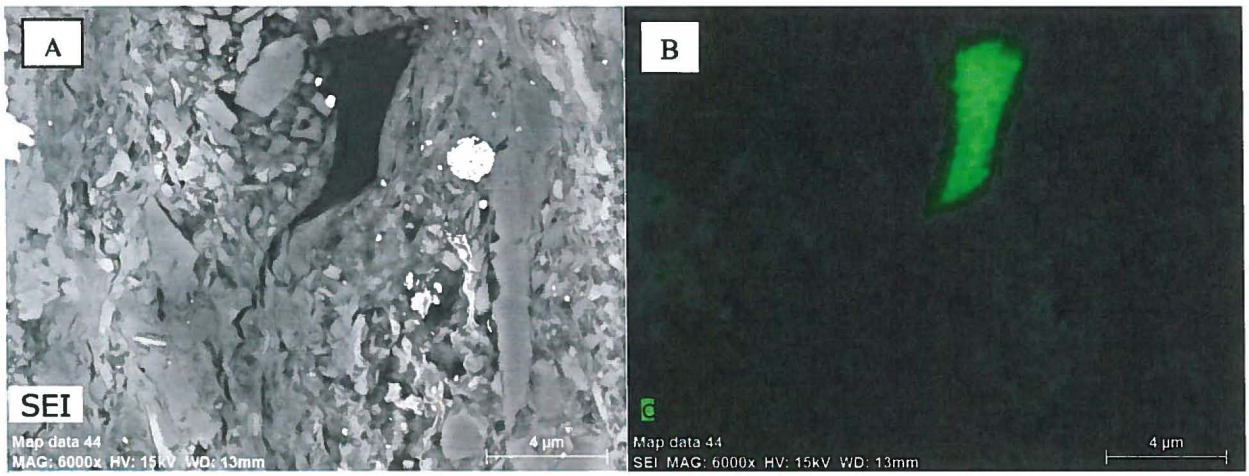

Figure A4. Organic carbon and pyrite in ion milled EF 29 sample. Figure (B) shows the EDS carbon map for picture (A) which shows the dark area to be carbon rich.

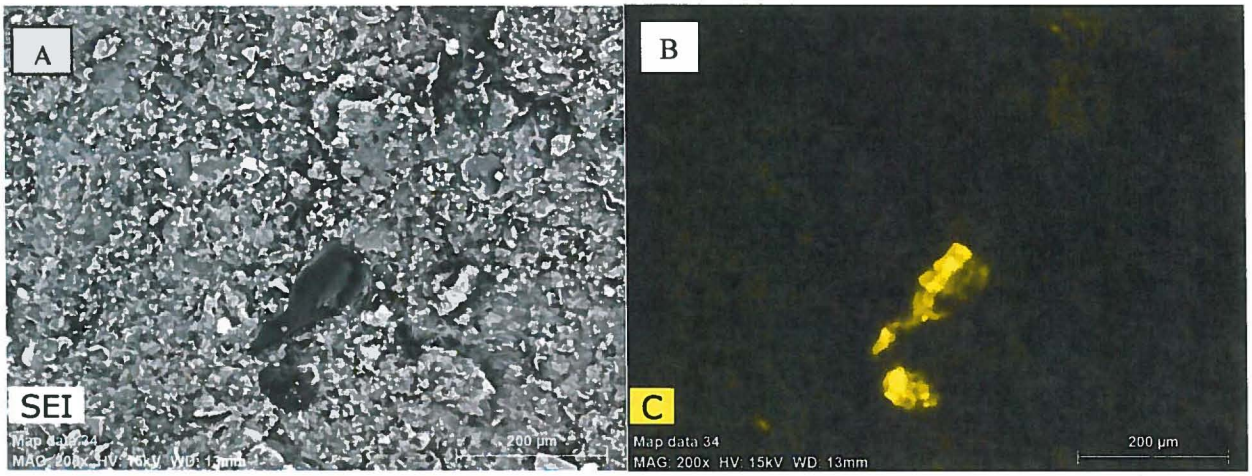

Figure A5. Another organic carbon in EF 29 visible after ion milled. Figure (B) is the EDS carbon color map for picture (A) . These images were both taken with the SEM.